JOURNAL OF THE MECHANICAL BEHAVIOR OF BIOMEDICAL MATERIALS 59 (2016) 197–206

Available online at www.sciencedirect.com

ScienceDirect

www.elsevier.com/locate/jmbbm

Research Paper

Streptococcus mutans biofilm transient viscoelastic fluid behaviour during high-velocity microsprays

S. Fabbri[a,*], D.A. Johnston[b], A. Rmaile[c], B. Gottenbos[c], M. De Jager[c], M. Aspiras[d], M.E. Starke[e], M.T. Ward[e], P. Stoodley[a,f]

[a]National Centre for Advanced Tribology at Southampton (nCATS), University of Southampton, Southampton SO17 1BJ, UK
[b]Biomedical Imaging Unit, School of Medicine, University of Southampton, Southampton SO16 6YD, UK
[c]Philips Research, High Tech Campus, Eindhoven 5656 AE, The Netherlands
[d]Wrigley, Chicago, IL 60613, USA
[e]Philips Oral Healthcare, Bothell, WA 98021, USA
[f]Department of Microbial Infection and Immunity and the Department of Orthopaedics, Centre for Microbial Interface Biology, The Ohio State University, Columbus, OH 43210, USA

ARTICLE INFO

Article history:
Received 18 August 2015
Received in revised form
12 December 2015
Accepted 14 December 2015
Available online 23 December 2015

Keywords:
Biofilm
Oral hygiene
High-speed camera
Fluid dynamics
Mechanical properties
Viscoelasticity

ABSTRACT

Using high-speed imaging we assessed *Streptococcus mutans* biofilm–fluid interactions during exposure to a 60-ms microspray burst with a maximum exit velocity of 51 m/s. *S. mutans* UA159 biofilms were grown for 72 h on 10 mm-length glass slides pre-conditioned with porcine gastric mucin. Biofilm stiffness was measured by performing uniaxial-compression tests. We developed an in-vitro interproximal model which allowed the parallel insertion of two biofilm-colonized slides separated by a distance of 1 mm and enabled high-speed imaging of the removal process at the surface. *S. mutans* biofilms were exposed to either a water microspray or an air-only microburst. High-speed videos provided further insight into the mechanical behaviour of biofilms as complex liquids and into high-shear fluid–biofilm interaction. We documented biofilms extremely transient fluid behaviour when exposed to the high-velocity microsprays. The presence of time-dependent recoil and residual deformation confirmed the pivotal role of viscoelasticity in biofilm removal. The air-only microburst was effective enough to remove some of the biofilm but created a smaller clearance zone underlying the importance of water and the air–water interface of drops moving over the solid surface in the removal process. Confocal and COMSTAT analysis showed the high-velocity water microspray caused up to a 99.9% reduction in biofilm thickness, biomass and area coverage, within the impact area.

*Correspondence to: National Centre for Advanced Tribology at Southampton (nCATS), Faculty of Engineering and the Environment, University of Southampton, Southampton SO17 1BJ, UK.
E-mail address: stefaniafabbri1987@gmail.com (S. Fabbri).

http://dx.doi.org/10.1016/j.jmbbm.2015.12.012
1751-6161/

1. Introduction

Dental plaque biofilms are the heterogeneous bacterial communities attached to teeth and soft tissues and embedded in a matrix composed mainly of extracellular DNA, proteins, and polysaccharides (Marsh and Bradshaw, 1995). Oral biofilms are associated with the development of caries, gingivitis and periodontitis (Costerton et al., 1995; Donlan and Costerton, 2002). Dental caries occurs through the dissolution of the enamel by acidogenic bacteria such as *Streptococcus mutans*, *Streptococcus sobrinus*, and lactobacilli (Featherstone, 1999). Biofilm complex structure makes dental diseases difficult to control and to eradicate, thus becoming a worldwide public health problem (Selwitz et al., 2007). When biofilms are subjected to different flow conditions, they mechanically behave as viscoelastic fluids (Klapper et al., 2002; Peterson et al., 2015; Towler et al., 2003; Wilking et al., 2011). This means that at low-shear rates biofioms have a "solid-like" behaviour and are able to store energy, while at high-shear rates they become "fluid-like" and lose their ability to store elastic energy. Energy dissipation through viscoelasticity is an important characteristic because it allows biofilms to tolerate rapidly-changing shear stresses without detaching from the surface. In dentistry, fluid shear stresses generated via either non-contact toothbrushing or fluid flow play a major role in biofilm detachment (Hope et al., 2003; Hope and Wilson, 2003; Paramonova et al., 2009) since dental plaque mainly accumulates in particular areas inside the mouth (such as pits, fissures, interproximal (IP) spaces and subgingival areas) inaccessible for toothbrush bristles and dentifrices (Fried, 2012). Therefore, the understanding of biofilm mechanical properties under various hydrodynamic flows represents an important part for the design of more effective strategies to remove and to control dental plaque biofilms. Oral irrigators, which generate a continuous pulsating or steady water jet designed to remove interdental and subgingival plaque are widely used as a supplement to toothbrushing, or to replace traditional flossing (Barnes et al., 2005; Jahn, 2010). More recently, mechanical biofilm removal either using low volume, high-velocity water droplets (Cense et al., 2006) or by entrained air bubbles (Parini and Pitt, 2006; Sharma et al., 2005b) has shown positive results due to the droplets' impact pressure, hydrodynamic shear stresses and the surface tension effects of the passage of an air–water interface over a solid surface (Busscher et al., 2010b).

In previous studies we grew *S. mutans* biofilms on and between two central incisors of a periodontal model to recreate the realistic geometry of the IP space (Rmaile et al., 2012). Then we performed high-speed imaging to assess biofilm removal and viscoelastic behaviour during the exposure to high-velocity microbursts (Rmaile et al., 2014). We also performed Computational Fluid Dynamics (CFD) simulations to predict wall shear stresses generated over the tooth surface during the burst (Rmaile et al., 2015). However, due to the opaque nature of the surface we could not see the details of biofilm removal process at the surface. Here we developed an in vitro IP model allowing the parallel insertion of two biofilm-colonized glass slides which could be monitored through the side of the slide by a high-speed camera. Biofilms were exposed to high-velocity water microsprays or air-only microbursts to assess the effects of these different fluid flows on the biofilm–burst interactions and biofilm viscolastic mechanical behaviour with respect to the removal process.

2. Materials and methods

2.1. Bacteria and growth media

Biofilms were inoculated with a *S. mutans* UA159 (ATCC 700610) adjusted overnight culture (10^6 cfu/mL) grown in a 2% sucrose-supplemented brain-heart infusion (BHI+S medium) (Sigma-Aldrich). Type II porcine gastric mucin (Sigma-Aldrich) was added to the BHI+S medium (BHI+SM medium). Petri plates or microscope glass slides were conditioned with 10 mL of the BHI+SM medium for 24 h to allow mucins to cover the surface. Then, biofilms were grown in static conditions for 72 h at 37 °C and 5% CO_2 with BHI+SM medium replacement every 24 h. We also grew biofilms on non-mucin conditioned plates and in BHI+S medium (control *S. mutans* biofilms) to assess the influence of mucin on the mechanical properties.

2.2. Uniaxial compression tests

Uniaxial compression experiments were performed on control *S. mutans* biofilms and on *S. mutans* biofilms grown on mucin-conditioned petri plates and with mucin-supplemented medium using an Electroforce 3200 testing instrument (Bose). Since biofilms are known to be viscoelastic materials and their mechanical behaviour varies with the strain rate applied, we performed uniaxial compression experiments at a constant rate of 0.05 mm/s. An upper cylindrical plunger of a diameter (D) of 7.75 mm compressed the biofilm and a 5 N capacity load cell (Honeywell Sensotec, Columbus, OH, USA) recorded the resulted force. Biofilm stiffness under constant strain rate was measured calculating the Young's modulus (E) from the stress–strain curves as previously described (Rmaile et al., 2012). Six independent replicate experiments were performed ($n=6$). Statistical analysis was performed using unpaired two samples t-test for normally distributed data and difference considered significant where $p<0.05$.

2.3. In vitro IP model and high-velocity microsprays

To allow high-speed camera imaging at the surface we developed an in vitro IP model (Fig. 1). The model consisted of a rectangular clear plastic holder, in which two grooves were made for the parallel insertion of two *S. mutans* biofilm-colonized slides at a distance of 1 mm. Slides were cut at 10 mm (10 mm-length slice) as a representative length, in the outside-in direction, of the proximal surface of the human molars. Since most of the biofilm was rapidly cleared from the 10 mm length of the slide we also grew *S. mutans* biofilms on full-length slides (75 mm × 25 mm) in order to more clearly assess the fluid nature of the biofilm which was most evident at the interface between the spray and the biofilm. Prior to the insertion into the IP model, the initial thickness of the

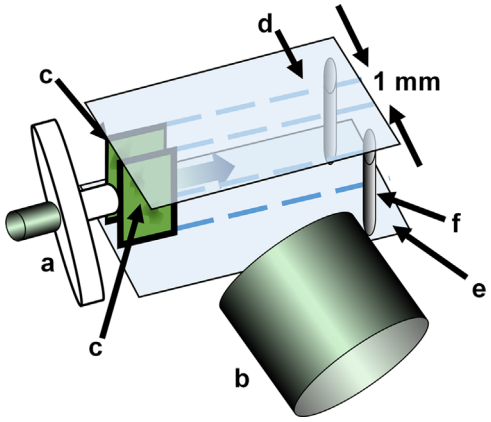

Fig. 1 – Schematic showing the juxtaposition of the IP model, the tip of the AirFloss (a) and the lens of the hyperspectral camera (b). The IP model was made up of two biofilm-colonized microscope slides (in green) (c) held in parallel grooves in top and bottom plates (d and e) to make a 1-mm gap. The slides length represented in this schematic is 10 mm. Two support pillars were placed at the back of the holder (f). The collar holding the AirFloss neck to the bottom plate (e) so that the tip was firmly abutted to the IP gap is not shown for clarity. The direction of the microspray though the IP space is indicated by the blue arrow. (For interpretation of the references to color in this figure legend, the reader is referred to the web version of this article.)

biofilm was 51.8±9.1 μm (mean±1 SD, $n=9$), measured by COMSTAT from 3D confocal images (see Section 2.6). A Philips Sonicare AirFloss HX8111 commercially available oral hygiene device was used to generate high-velocity microsprays. The device was filled either with water to generate a water microspray, as per normal use of the device, or was left empty in order to generate an air-only microburst.

2.4. *S. mutans biofilms exposure to high-speed microsprays*

The dental cleaning device was positioned in order to have the tip centred between the two biofilm-covered slides inside the IP model (Fig. 1). The shooting was recorded at 8000 frames per seconds (fps) with a high-speed camera MotionPro X3 (IDT) equipped with a Sigma 105 mm f/2.8 EX DG Macro lens. To characterize the hydrodynamic of the flow during the water microspray, high-speed images were also taken of the burst into open air.

2.5. *High-speed video post-processing*

The HSC videos were converted in Fiji (http://fiji.sc/Fiji) (Schindelin et al., 2012) to a stack with each frame in the stack being a different time (T) so that the volume could be represented as XYT co-ordinates. The external diameter of the nozzle tip ($d_{AF}=2$ mm) was used as an internal scale to calibrate pixels with microns.

In order to characterize the water microspray hydrodynamic, a water microspray average velocity (u) was defined as $u=\Delta X/\Delta T$ (1), where ΔX is the microspray length variation along the X axis and ΔT is the time interval between the two adjacent frames. A Reynolds number (Re) was also measured using the Reynolds equation for free jets:

$$\mathrm{Re}=\frac{u\rho D}{\mu} \quad (1)$$

where ρ and μ are the density (998 kg/m^3) and the viscosity (1.003×10^{-3} Pa s) of water at 20 °C and D is the Airfloss tip internal diameter (1 mm). Videos were analysed from five independent experiments ($n=5$).

Regarding biofilms exposure to high-speed microsprays, the area of the biofilm cleared zone caused by the microsprays (A) was measured as a function of the time in each frame every 5 ms. Using the Threshold function in Fiji only the cleared zone was selected in each frame. Then A was measured using the Measure function. Videos were analysed from three independent experiments ($n=3$). Statistical analysis was performed using unpaired two samples t-test for normally distributed data and difference considered significant where $p<0.05$.

Biofilm recoil was measured using the reslice function which creates a time-trace along a defined line. As the biofilm recoiled towards the cleared zone it makes a continuous curve from the left to the right. Biofilm total recoil was defined as the difference between the final and initial length. Videos were analysed from three independent experiments ($n=5$ measurements per repeat). Statistical analysis was performed using unpaired two samples t-test for normally distributed data and difference considered significant where $p<0.05$.

2.6. *Confocal and scanning electron microscope analysis*

The thickness of the control biofilms (unexposed to a spray or air jet) and those biofilms on the 1 cm slide immediately after the shooting were carefully transferred to petri plates filled with 1% (wt/vol) phosphate-buffered saline (PBS) solution (Sigma-Aldrich). Then, the samples were fixed by the addition of 100 μL of 4% (wt/vol) paraformaldehyde (PFA) solution (Agar Scientific) and left for 1 h inside the fridge. Afterwards, the biofilm slides were rinsed twice with 1% PBS in order to disrupt loosely-adherent bacteria. To visualize dead cells in the biofilm, slides were immersed in a 0.2% solution of Propidium iodide (PI, Live/Dead BacLight Bacterial Viability Kit, Invitrogen) for 30 min, washed three times with 1% PBS and then covered immediately with mowiol mounting medium (20 gr of mowiol powder, 88 mL of 1% PBS solution, 40 mL of Glycerol and 2.4 mL of 5% Citifluor solution). Mowiol mounting medium is not only optically appropriate (non-absorbing, containing no autofluorescence, or light scattering), but also has an anti-fade agent which is capable of reducing light-induced fading of the fluorophore. Immediately after, the samples slides were covered with a microscope coverslip and left in the fridge for 24 h in order to settle the mountant uniformly over the whole slide. Then, the samples were imaged using an inverted Leica DMI600 SP5 confocal scanning laser microscope (CSLSM, Leica Microsystems) using a HCX PL APO CS 63x/1.3 NA glycerol immersion lens. Three random confocal images were taken on each of three independent replicate control (not exposed to the

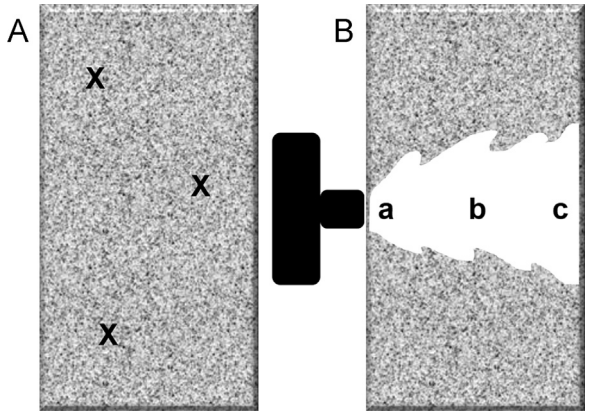

Fig. 2 – (A) Schematic illustrating a *S. mutans* biofilm covered slide (10 mm × 25 mm) prior the shooting. Three random confocal images (X) were taken on the non-exposed slide. (B) Schematic illustrating a *S. mutans* biofilm covered slide (10 mm × 25 mm) after the shooting. Confocal images were taken at 1 mm (a), 5 mm (b) and 8 mm (c) from the leading edge of the slide. Biofilm is depicted grey while the biofilm clearance zone white.

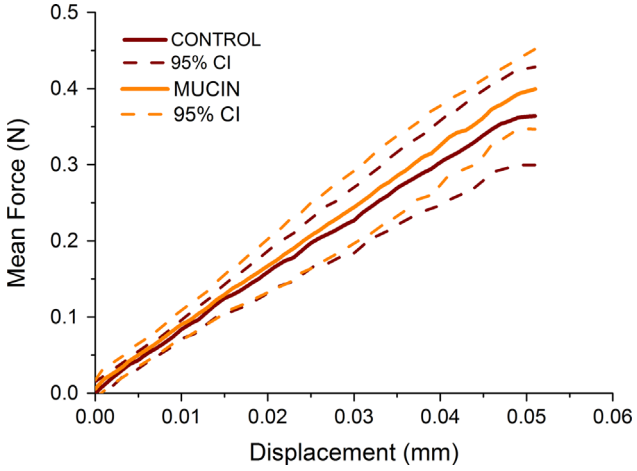

Fig. 3 – Load-versus-displacement curves of 3-days old *S. mutans* biofilms grown on mucin-conditioned plates or non-mucin conditioned plate from uniaxial compression experiments performed under a contant strain rate of 0.05 mm/s. The solid lines are the average of 5 mechanical tests and the dashed lines are the 95% confidence intervals.

spray) biofilm slides to establish the thickness of the biofilm prior to the shooting (Fig. 2A). For the independent triplicate spray-exposed biofilm slides, confocal images were taken inside the clearance zone, at 1, 5 and 8 mm distances directly downstream from the nozzle, from the leading edge of the slide (Fig. 2B). Thus the experiments were replicated three times with triplicate repeated confocal images for each position within each replicate.

The amount of biofilm removed by the water microspray was quantified by comparing biofilm thickness (T), surface area (A) and biomass (B) of non-exposed control slides and slides after the shooting by analysing the confocal images with the Matlab plugin COMSTAT (Heydorn et al., 2000). The percent reduction in biofilm thickness (%RT), biomass (%RB) and surface area (%RA) were also measured as:

$$\%\mathrm{RT} = \frac{T_0 - T_{CZ}}{T_0} \times 100 \quad (2)$$

$$\%\mathrm{RB} = \frac{B_0 - B_{CZ}}{B_0} \times 100 \quad (3)$$

$$\%\mathrm{RA} = \frac{A_0 - A_{CZ}}{A_0} \times 100 \quad (4)$$

where T_0, B_0, A_0 and T_{CZ}, B_{CZ}, A_{CZ} are biofilm thickness, surface area and biomass prior the and after the shooting respectively.

We compared the thickness of the control (un-shot) biofilm with that at each of these distances using a t-test on an $n=3$ for the control and an $n=3$ for the experiment biofilms. In addition we did a t-test to establish that there was no significant difference between the biofilm thicknesses at the three different distances from the nozzle after shooting ($P>0.05$) and so also grouped these values to compare the mean thickness within the cleared area with that of the thickness in the unexposed control biofilm ($n=9$).

A Scanning Electron Microscope (SEM, FEI Quanta-200) was also used to qualitatively assess biofilm removal in high resolution.

3. Results

3.1. *S. mutans* biofilm structure and mechanical properties

The biofilm structure was similar to that reported previously (Rmaile et al., 2014, 2012) and consisted of a dense base layer of cells interspersed with prominent clusters separated by water channels. At 3 days, the unexposed *S. mutans* biofilm was 51.8±4.9 μm ($n=9$) thick. The load–displacement curves under constant strain rate showed a linear behaviour (Fig. 3) with a Young's modulus of 760±201 kPa for the mucin grown biofilm and 800±200 kPa for the non-mucin grown biofilm. These differences were not significant ($p<0.05$, $n=6$).

3.2. *High-velocity water microspray hydrodynamics*

High-speed videos of the water microspray into air showed two distinct phases (**Supplemental** Movie 1). The first phase was a 10.5 ms (±0.3 ms, $n=5$) water jet, while the second phase was a 45.9 ms (±0.8 ms, $n=5$) water spray (Fig. 4A). The total microspray time interval (Δt) was 56.8 ms (±0.6 ms, $n=5$). For the jet phase, the water microspray average velocity (u) started from a value of 36.6 m/s (±6.2 m/s, $n=5$) and decreased to a minimum value of 31.7 m/s (±6.8 m/s, $n=5$) before increasing to a maximum value of 51.1 m/s (±6.3 m/s, $n=5$) (Fig. 4B). The exit-velocity profile of the spray phase was less variable over time, and started from a maximum of 12.9 m/s (±1.7 m/s, $n=5$) decreasing to 10.9 m/s (±3.9 m/s, $n=5$). The Re number calculated for the jet phase ranged from 30,000 to 50,000 predicting fully-developed turbulent flow.

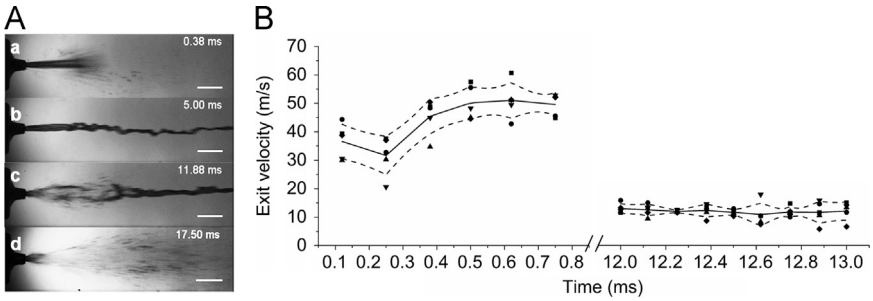

Fig. 4 – (A) Individual frames from a high-speed camera video of the AirFloss water microspray as a free-jet into air at different time points. (a) Initiation of the burst. (b) Fully-developed jet phase. (c) Transition phase from water jet to water spray. (d) Spray phase. Scale bar=5 mm. (B) Water microspray exit velocity as a function of the time for the first part of the jet phase (0–0.8 ms) and the spray phase (12–13 ms). The solid lines is the average exit velocity and the dashed lines are 95% confidence intervals. Individual data from 5 independent runs shown as various symbols.

3.3. *S. mutans* biofilm transient viscoelastic fluid behaviour

High-speed videos of biofilms exposed to high-velocity microsprays revealed that the water microspray and the air-only microburst rapidly entered the IP channel pushing the biofilm outwards towards the distal end of the slide, creating a biofilm cleared zone. The microsprays appeared to cause the biofilms to liquefy and flow over the slide in an extremely short period of time (<60 ms). We observed wave-like structures forming at the biofilm/fluid interface for the entire burst duration (Fig. 5A and **Supplemental** Movie2). Also vortices were seeing developing in a very short time (<5 ms) at the edges of the remaining biofilm (Fig. 5B and **Supplemental** Movie 3). When the microspray ended, these structures disappeared and left no trace of their formation on the slide surface, suggesting biofilm fluidisation can be an extremely transient mechanical behaviour.

Biofilm fluid behaviour was also observed at the edge of the microscope slides where biofilm was seen dripping out and creating droplets which where pushed out of the IP space (Fig. 6 and **Supplemental** Movie 4). Biofilm drops were seen first stretching and then breaking off.

Immediately after the microspray ended, the biofilms exhibited viscoelastic behaviour by undergoing a time-dependant elastic recoil, which caused a the reduction in the width of the cleared channel (Fig. 7A and **Supplemental** Movie 5). Reslice graphs showed an exponential increase in biofilm elongation (recoil) across the spray direction (Fig. 7B). The rate of recoil was similar to that of a viscoelastic creep recovery (Towler et al., 2003). Biofilm total recoil was 0.41 mm ($\pm$0.22, n=15 from three independent replicates) in aproximately 15 ms.

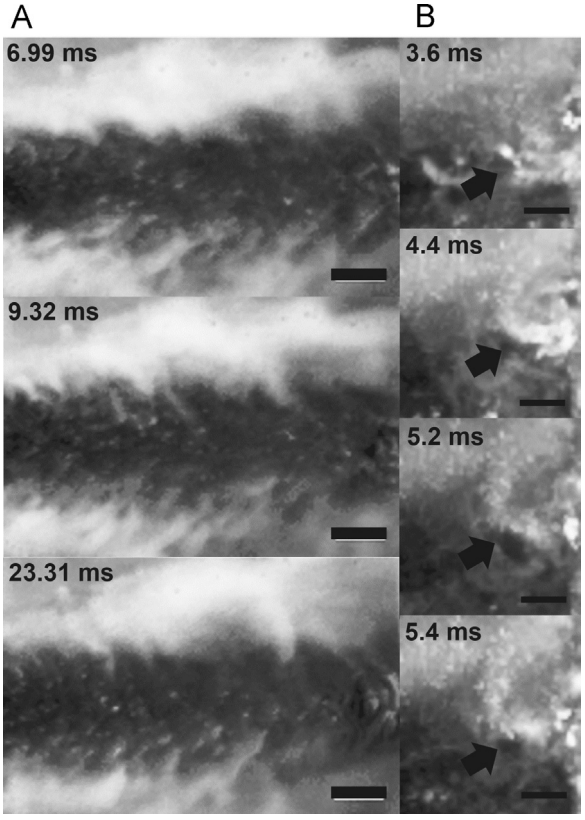

Fig. 5 – Cropped areas from individual frames from two high-speed camera videos showing *S. mutans* biofilm fluid behaviour when exposed to a high-velocity water microspray. The *S. mutans* biofilmappeared whitish grey and the clearance zone was black. The flow was left to right. The microspray caused the transient formation of wave-like patterns (A) or vortices (B) at the biofilm/fluid interface. Scale bars are 1 mm and 0.5 mm for panels A and B respectively.

3.4. *S. mutans* biofilm removal

High-speed camera videos of *S. mutans* biofilms removal from the 1-cm length slides showed a different removal process when exposed to a water microspray or an air-only microburst (Fig. 8A–C and **Supplemental** Movie 6 and Movie 7). Biofilm cleared area caused by the water microspray initial "jet" phase ($\Delta t \sim 10$ ms) created a relatively straight channel through the biofilm clearing an area of 32.6 mm^2 ($\pm$6.3 mm^2, n=3) at a constant rate of removal. In the second "spray" phase ($\Delta t \sim 45$ ms) the zone of clearance flared out thus that a further area of 8.2 mm^2 ($\pm$2.1 mm^2, n=3) was removed over an additional 20 ms. There was little further clearance over the remaining 25 ms of the burst. A total area of 40.8 mm^2 ($\pm$0.9 mm^2, n=3) was cleared of biofilm at the end of the water microspray ($\Delta t \sim 55$ ms). In contrast, the air-only

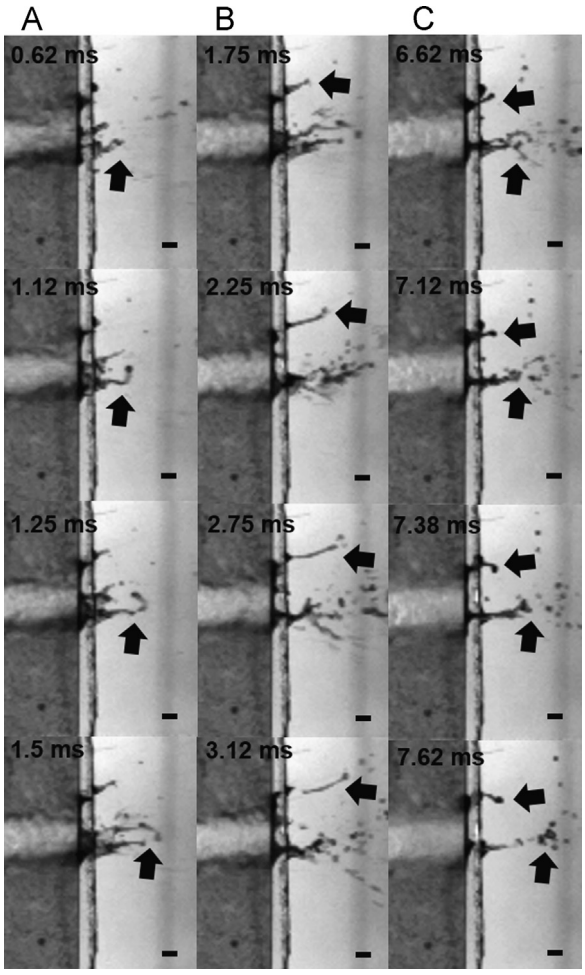

Fig. 6 – Cropped area from individual frames from a high-speed camera video showing three different sequences (A, B and C) of *S. mutans* biofilm fluid behaviour during the exposure to an air-only microburst. The flow was left to right. As the biofilm was pushed out of the IP space, it formed droplets which first elongated and then broke off (white arrows). Scale bar is 1 mm.

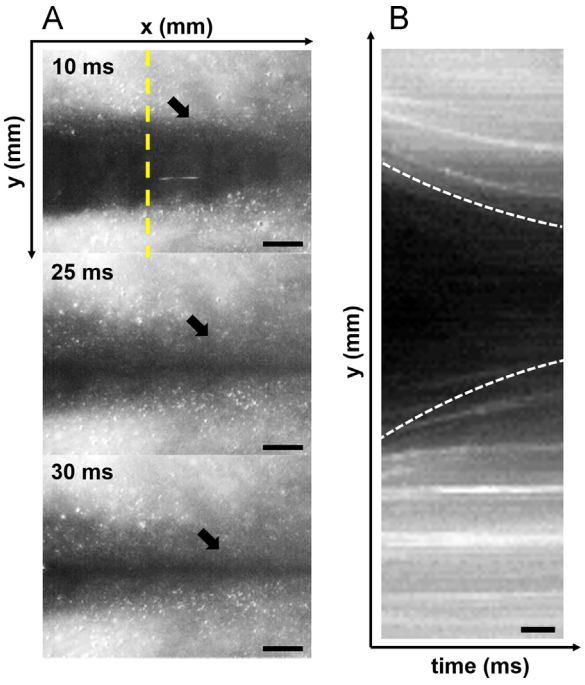

Fig. 7 – Images from a high-speed camera video showing biofilm viscoelastic recoil after a the air-only microburst spray. (A) Subsequent frames show the biofilm move back into back into the previously cleared channel. Scale bar=1 mm. (B) Time trace using the FIJI "reslice function" taken perpendicularly across the cleared channel (indicated by the yellow dashed line in panel (A) showing the time-dependant biofilm recoil. Scale bar=10 mm. The recovery of back into the cleared channel from both sides of the channel is indicated by the white-dashed lines and appears similar to that of an exponential decay function characteristic of viscoelastic creep recovery. (For interpretation of the references to color in this figure legend, the reader is referred to the web version of this article.)

microburst only generated a straight channel through the biofilm, with less biofilm being "forced" off the edge of the slide, resulting in a cleared area of $11.7 \pm 0.9\ mm^2$ after approximately 30 ms (Fig. 8D). The final biofilm clearance zone generated by the water microspray was approximately 20 times greater than the one created by the air-only microburst ($p<0.05$, $n=3$).

3.5. *Microscopic evaluation of biofilm removal*

SEM micrographs of biofilms grown on a 1-cm length slide and exposed to a single microburst revealed a clearance zone with well-defined edges (Fig. 9A). Higher magnification revealed that there were some small clusters and single bacterial cells remaining on the surface in the centre of the cleared area. Confocal micrographs were in agreement with SEM images and allowed the remaining biofilm to be quantified from the 3D stack (Fig. 9B).

Quantification of *S. mutans* biofilms removal in the exposed area caused by the high-speed water microspray showed a significant reduction in terms of thickness, biomass and surface area compared to the unshot sample (Table 1). No statistical difference was observed between the 1 mm, 5 mm and 8 mm positions in terms of biofilm thickness, biomass and area coverage ($p<0.05$, $n=3$). Therefore we measured thickness, biomass and surface area in the exposed zone by grouping together the data from the different positions ($n=9$ from three independent replicates).

4. Discussion

The in vitro IP model successfully simulated a simplified geometry of an interproximal biofilm and allowed high-speed imaging of the biofilm on the surface during the shooting. We are aware that this model represents a departure from a dental clinical relevant model; however, it allowed us to add a direct real-time biofilm imaging at the surface to the previous tests on typodonts (Rmaile et al., 2015', 2014). In particular, here we show that high-speed microsprays caused biofilm

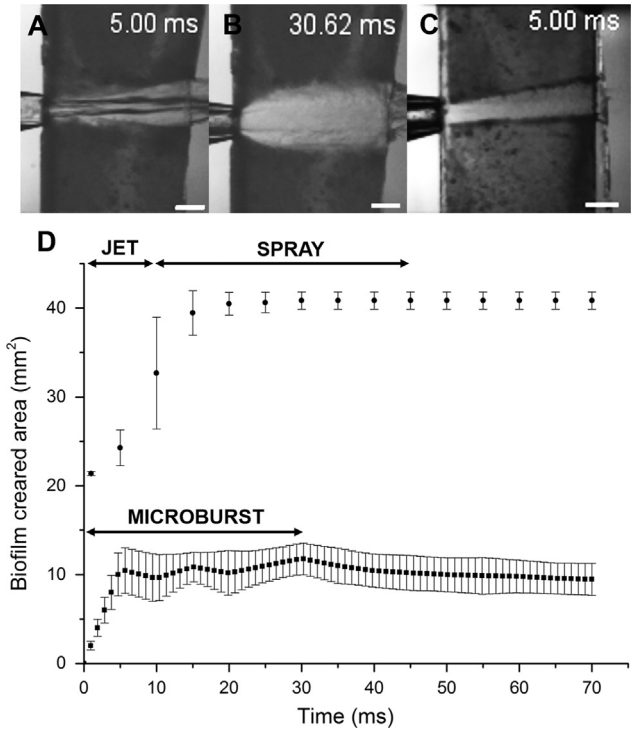

Fig. 8 – Individual frames showing *S. mutans* biofilm exposure to a high-speed water microspray (A and B) or air-only microburst (C) into the IP model space. Frames show *S. mutans* biofilm-colonized slide proximal to the camera (biofilm depicted as dark grey and biofilm clearance zone depicted as white). The AirFloss nozzle tip was located at the left edge of the slide. (A) Jet phase creating a straight clearance zone. (B) Spray phase generating a conical clearance zone. (C) Air-only microburst generating a straight clearance zone. Scale bar=2 mm. (D) Mean biofilm cleared area as a function of the time during the water microspray (dots) and the air-only microburst (squares). Data points represent the mean of triplicate experimental repeats with standard error bars. Data were statistically different in each time point ($p<0.05$, $n=3$).

fluidisation on the surface in a highly transient manner (Figs. 5 and 6). This phenomenon was extremely quick (<60 ms) and cannot be seen with regular videography or microscopic imaging techniques. Biofilm fluidification can be the result of mixing processes occurring between the water and the biofilm structure. Since high Re numbers measured for the water-jet phase suggested turbulent behaviour, it might be possible that the vortices observed at the edges of the remaining biofilm can be turbulent eddies. Turbulent mixing together with biofilm fluid behaviour could possibly enhance the mass transfer inside the unremoved biofilm. This phenomenon could, in future, help antimicrobial delivery inside dental biofilms for a better therapeutical effect. In the oral cavity, dental biofilm removal under non-contact brushing is subjected to different shear forces which can cause an expansion in the structure of unremoved biofilms due to its viscoelastic nature (Busscher et al., 2010a; Peterson et al., 2015). Investigators demonstrated that fluid-dynamic activity generated by power toothbrushes can change biofilm viscoelastic properties which in turn enhance antimicrobials penetration inside the remaining biofilm (He et al., 2014; Sjogren et al., 2004; Stoodley et al., 2007).

In addition to fluid behaviour we also demonstrated biofilm viscoelastic behaviour showing biofilm time-dependent recoil and residual strain when the shear-stress caused by the microsprays was removed (Fig. 7). Other studies have reported that biofilms exhibit both elastic recoil and residual strain caused by viscous flow (Klapper et al., 2002; Rupp et al., 2005; Shaw et al., 2004; Towler et al., 2003). Conventional "before" and "after" imaging would not have revealed this behaviour and the drawn conclusion would be that a device had failed to remove biofilm from the surface in the first place. Thus, when dealing with dental biofilm removal, the shear forces should be high enough and sustained for a sufficient time to overcome the recoil effect and be able to detach the biofilm completely off the surface.

It is known from the literature that *S. mutans* specifically bind salivary mucins present in the dental pellicle which cover the tooth surface (Gibbons and Hay, 1989). Therefore, we added type II porcine gastric mucin to the biofilm growth medium as a substitute for salivary mucin (Kolenbrander, 2011). The we conditioned microscope slides with the mucin medium prior the inoculation in order to simulate *S. mutans*/mucin interactions. We then performed uniaxial compression test to assess how mucin in the medium might influence biofilm mechanical properties and thus biofilm behaviour. Although mucins have been shown to be important in the adhesion of *S. mutans*, in both promoting attachment (Kishimoto et al., 1989) or inhibiting attachment and biofilm formation (Frenkel and Ribbeck, 2015; Marsh et al., 2009) we found the presence of mucin as a slide preconditioned pellicle or in the growth medium had no significant effect on rigidity ($p>0.05$), suggesting that it did not influence matrix production, or was not incorporated at all into the matrix. It is important to mention that mucin in the growth medium was a simplified model of the dental pellicle. Human saliva contains not only mucins but a complex mixture of proteins, electrolytes and antibacterial compounds. For our work we used commercially available mucin since it is more consistent and easier to work with than high viscosity human saliva, but in order to have a more complete picture, mechanical experiments should be performed with human saliva as the growth medium. However, we also discovered that increasing the growth period from 2 days in previous studies (Rmaile et al., 2012) to 3 days significantly increased the rigidity of the biofilm from 0.280 kPa to 760 kPa, a factor of $\sim 10^3$. This is consistent with findings showing that the elastic modulus of dental biofilms is positively correlated with the amount (and density) of matrix components (Hwang et al., 2014; Klein et al., 2015; Waters et al., 2013), and stresses the importance of frequent and consistent oral hygiene to continually remove and disrupt plaque biofilm before it gets stiffer.

The initial jet phase blasted a channel through the biofilm and the second spray phase extended the zone of clearance, thus the combination of these two phases appear complimentary. The water microspray cleared proximally four times of the area of biofilm than the air-only microburst ($p<0.05$) (Fig. 8B). Although interestingly the force of the air alone was strong enough to remove some biofilm. This suggests that

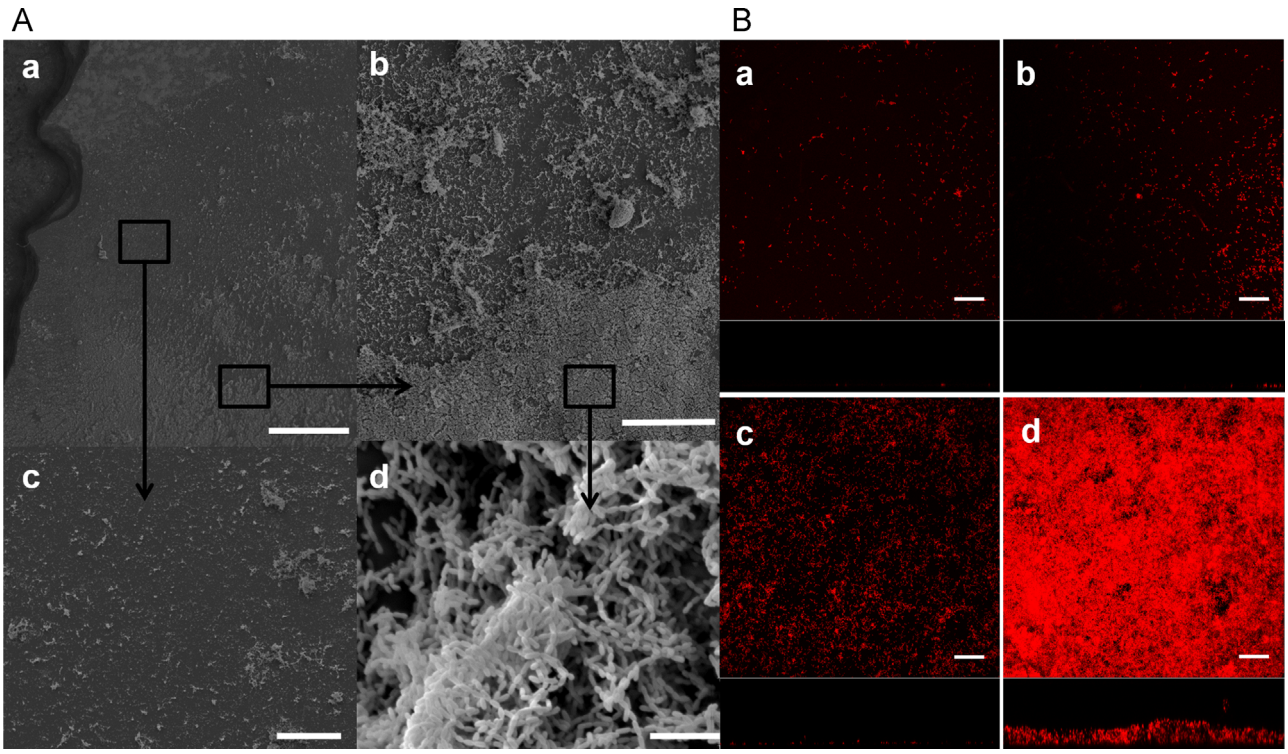

Fig. 9 – (A) Scanning electron microscopy images of a representative slide exposed to a single water microspray burst. (a) Lower magnification of the clearance zone. The leading edge of the slide was located at the left as presented in Fig. 2. Scale bar=500 μm. (b) Higher magnification SEM of the edge delimiting the clearance zone showing a reduction of biofilm but with remaining clusters and single cells. Scale bar=100 μm. (c) Inside the clearance zone only small clusters and single cells remained. Scale bar=100 μm. (d) Biofilm composed of dense clusters and chains of cocci in the unexposed area away from the microburst. Scale bar=50 μm. (B) Confocal images in *x*–*y* plan view with *x*–*z* cross section below at distances of (a) 1 mm, (b) 5 mm and (c) 8 mm from the microspray inlet (see Fig. 2). (d) An image of the biofilm in an unexposed area. Scale bar=100 μm.

Table 1 – Thickness, biomass, surface area and relative percent reductions of *S. mutans* biofilms prior and after the high-speed microspray exposure. Experimental data reported as mean and 1 standard deviation. Values marked in bold were statistically different from the unexposed controls ($p<0.05$).

Sample	Location	Thickness (μm)	Biomass ($\mu m^3/\mu m^2$)	Area ($10^5 \times \mu m^2$)	RT (%)	RB (%)	RA (%)
Unexposed control	Random ($n=9$)	51.79±9.01	28.53±5.86	0.41±0.14	–	–	–
Exposed	1 mm from nozzle ($n=3$)	0.38±0.49	0.25±0.29	0.11±0.10	99.2±0.9	99.1±1.0	99.4±0.4
	5 mm from nozzle ($n=3$)	0.03±0.03	0.03±0.02	0.25±0.21	99.9±0.1	99.9±0.1	99.7±0.2
	8 mm from nozzle ($n=3$)	0.13±0.14	0.07±0.06	41.05±13.22	99.7±0.26	99.7±0.2	99.3±0.5
	Combined ($n=9$)	0.16±0.24	0.10±0.15	0.20±0.15	99.7±0.5	99.6±0.5	99.5±0.4

water inside the microspray plays a crucial role in the detachment mechanisms possibly because of the higher shear stresses caused by the more viscous water drops as well as the surface tension effect of the moving air–water interface of the drop over the biofilm-colonized surface (Sharma et al., 2005a). Previous studies demonstrated that, when water shear stresses inside flow cells reached a critical value between 5 and 12 Pa, biofilm macroscopic clusters detached from the surface (Ohashi and Harada, 1994; Stoodley et al., 2002). Although high-speed camera videos of the water microspray developing inside the IP space model demonstrated the complexity and the turbulence of the flow (**Supplementary** Movie 1), we made a rough estimate of the magnitude of the shear stresses (τ_w) acting over the surface of the biofilm for the water microspray first phase (i.e. water jet) and the air-only microburst, making two simplifying assumptions: a) when bursts developed inside the channel formed by the two *S. mutans* biofilm slides, the biofilm exposed area can be approximated to a square channel having a depth and a width of 1 mm; b) the air-only microburst had the same maximum velocity as the water jet (51.1 m/s). The corresponding wall shear stresses values were 7.4 kPa and 0.016 kPa for the water microspray and air-only microburst, respectively. These results were consistent with the values found by Rmaile et al. (2014) where a computed $\tau_w=3$ kPa was required to remove 95% of the biofilm by shooting water micro-drops from a prototype AirFloss at a velocity of 60 m/s. Quantification of *S. mutans* biofilm removal in different positions along the 10-mm slide showed a reduction in biofilm thickness, biomass and area covelage up to 99.9% (Table 1), similar to our previous studies (Rmaile, 2015', 2014', 2012). We are aware that one of the limitations of

confocal analyisis is that it is limited in being able to map in high resolution over larger areas. In this case the relevant areawould be that of the tooth surface in the IP space which will be on the order of 0.5–1 cm^2. Future work will considere Optical Coherence Tomography would as a complimentary technology to achieve both high resolution and a more complete mapping of the zone of clearance.

SEM images indicated that there was still some biofilm remaining in the clearance zone (Fig. 9A), underlining the importance of the adhesive viscoelastic forces which develop between the biofilm and the surface. Similar findings were obtained in a recent study on shear-induced detachment of 64 h *S. mutans* biofilms which showed a decrease in the biomass removal rate close to the surface because of the presence of a dense layer of EPS (Hwang et al., 2014). In addition, the authors also demonstrated that biofilm treated with EPS-digesting dextranase were easier to detach. Therefore, a possible new therapeutical approach can be the combination of high-speed fluid forces with specific matrix-digesting agents that facilitate the mechanical cleaning of dental biofilms.

5. Conclusions

High-speed videography revealed that high-velocity fluid-biofilm interactions can cause the biofilm to behave like a viscoelastic fluid over very short times-scales (ms). The ability of the biofilm to liquefy and flow over surfaces when exposed to mechanical forces is an important consideration in the future designs of oral hygiene devices. It also opens new opportunities to exploit this phenomenon with the aim of enhancing transport of dentifrices inside dental biofilms for increasing antimicrobials or anticaries therapeutical effects.

Acknowledgements

This work was financially funded in part by EPSRC DTP EP/K503130/1 award and in part by Philips Oral Helathcare, Bothell, WA, USA. M. Starke and M. Ward are employed by Philips Oral Healthcare, Bothell, WA, USA. The other authors declare no potential conflicts of interest with respect to the authorship and/or publication of this article. We also thank Dr. Janice M. Barton and Dr. Marco Longana from the Testing and Structures Research Laboratory (TSRL, University of Southampton) for providing the high-speed camera set up. All data supporting this study are openly available from the University of Southampton repository at http://dx.doi.org/10.5258/SOTON/384985.

REFERENCES

Barnes, C.M., Russell, C.M., Reinhardt, R.A., Payne, J.B., Lyle, D.M., 2005. Comparison of irrigation to floss as an adjunct to tooth brushing: effect on bleeding, gingivitis, and supragingival plaque. J. Clin. Dent. 16, 71.

Busscher, H., Jager, D., Finger, G., Schaefer, N., Van der Mei, H., 2010a. Energy transfer, volumetric expansion, and removal of oral biofilms by non-contact brushing. Eur. J. Oral Sci. 118, 177–182.

Busscher, H.J., Jager, D., Finger, G., Schaefer, N., Van der Mei, H.C., 2010b. Energy transfer, volumetric expansion, and removal of oral biofilms by non-contact brushing. Eur. J. Oral Sci. 118, 177–182.

Cense, A.W., Van Dongen, M.E.H., Gottenbos, B., Nuijs, A.M., Shulepov, S.Y., 2006. Removal of biofilms by impinging water droplets. J. Appl. Phys. 100 124701-124701-124708.

Costerton, J.W., Lewandowski, Z., Caldwell, D.E., Korber, D.R., Lappin-Scott, H.M., 1995. Microbial biofilms. Annu. Rev. Microbiol. 49, 711–745.

Donlan, R.M., Costerton, J.W., 2002. Biofilms: survival mechanisms of clinically relevant microorganisms. Clin. Microbiol. Rev. 15, 167–193.

Featherstone, J.D.B., 1999. Prevention and reversal of dental caries: role of low level fluoride. Community Dent. Oral Epidemiol. 27, 31–40.

Frenkel, E.S., Ribbeck, K., 2015. Salivary mucins protect surfaces from colonization by cariogenic bacteria. Appl. Environ. Microbiol. 81, 332–338.

Fried, J.L., 2012. Interdental cleansing. Access 2, 22–25.

Gibbons, R., Hay, D., 1989. Adsorbed salivary acidic proline-rich proteins contribute to the adhesion of *Streptococcus mutans* JBP to apatitic surfaces. J. Dent. Res. 68, 1303–1307.

He, Y., Peterson, B.W., Ren, Y., van der Mei, H.C., Busscher, H.J., 2014. Antimicrobial penetration in a dual-species oral biofilm after noncontact brushing: an in vitro study. Clin. Oral Investig. 18, 1103–1109.

Heydorn, A., Nielsen, A.T., Hentzer, M., Sternberg, C., Givskov, M., Ersbøll, B.K., Molin, S., 2000. Quantification of biofilm structures by the novel computer program COMSTAT. Microbiology 146, 2395–2407.

Hope, C.K., Wilson, M., 2003. Effects of dynamic fluid activity from an electric toothbrush on in vitro oral biofilms. J. Clin. Periodontol. 30, 624–629.

Hope, C.K., Petrie, A., Wilson, M., 2003. In vitro assessment of the plaque-removing ability of hydrodynamic shear forces produced beyond the bristles by 2 electric toothbrushes. J. Periodontol. 74, 1017–1022.

Hwang, G., Klein, M.I., Koo, H., 2014. Analysis of the mechanical stability and surface detachment of mature *Streptococcus mutans* biofilms by applying a range of external shear forces. Biofouling 30, 1079–1091.

Jahn, C.A., 2010. The dental water jet: a historical review of the literature. Am. Dent. Hyg. Assoc. 84, 114–120.

Kishimoto, E., Hay, D.I., Gibbons, R.J., 1989. A human salivary protein which promotes adhesion of *Streptococcus mutans* serotype c strains to hydroxyapatite. Infect. Immun. 57, 3702–3707.

Klapper, I., Rupp, C.J., Cargo, R., Purvedorj, B., Stoodley, P., 2002. Viscoelastic fluid description of bacterial biofilm material properties. Biotechnol. Bioeng. 80, 289–296.

Klein, M., Hwang, G., Santos, P., Campanella, O., Koo, H., 2015. *Streptococcus mutans*-derived extracellular matrix in cariogenic oral biofilms. Front. Cell. Infect. Microbiol. 5, 5.

Kolenbrander, Paul, E., 2011. Multispecies communities: interspecies interactions influence growth on saliva as sole nutritional source. Int. J. Oral Sci. 3.2, 49–54.

Marsh, P.D., Bradshaw, D.J., 1995. Dental plaque as a biofilm. J. Ind. Microbiol. 15, 169–175.

Marsh, P.D., Martin, M.V., Lewis, M.A., Williams, D., 2009. Oral Microbiology. Elsevier Health Sciences.

Ohashi, A., Harada, H., 1994. Adhesion strength of biofilm developed in an attached-growth reactor. Water Sci. Technol. 29, 281–288.

Paramonova, E., Kalmykowa, O.J., van der Mei, H.C., Busscher, H.J., Sharma, P.K., 2009. Impact of hydrodynamics on oral biofilm strength. J. Dent. Res. 88, 922–926.

Parini, M.R., Pitt, W.G., 2006. Dynamic removal of oral biofilms by bubbles. Colloids Surf. B: Biointerfaces 52, 39–46.

Peterson, B.W., He, Y., Ren, Y., Zerdoum, A., Libera, M.R., Sharma, P.K., van Winkelhoff, A.-J., Neut, D., Stoodley, P., van der Mei, H.C., 2015. Viscoelasticity of biofilms and their recalcitrance to mechanical and chemical challenges. FEMS Microbiol. Rev. 39, 234–245.

Rmaile, A., Carugo, D., Capretto, L., Aspiras, M., De Jager, M., Ward, M., Stoodley, P., 2014. Removal of Interproximal dental biofilms by high-velocity water microdrops. J. Dent. Res. 93, 68–73.

Rmaile, A., Carugo, D., Capretto, L., Zhang, X., Wharton, J.A., Thurner, P.J., Aspiras, M., Ward, M., Stoodley, P., 2012. Microbial tribology and disruption of dental plaque bacterial biofilms. Wear 306, 276–284.

Rmaile, A., Carugo, D., Capretto, L., Wharton, J.A., Thurner, P.J., Aspiras, M., Ward, M., De Jager, M., Stoodley, 2015. An experimental and computational study of the hydrodynamics of high-velocity water microdrops for interproximal tooth cleaning. J. Mech. Behav. Biomed. Mater. 46, 148–157.

Rupp, C.J., Fux, C.A., Stoodley, P., 2005. Viscoelasticity of *Staphylococcus aureus* biofilms in response to fluid shear allows resistance to detachment and facilitates rolling migration. Appl. Environ. Microbiol. 71, 2175–2178.

Schindelin, J., Arganda-Carreras, I., Frise, E., Kaynig, V., Longair, M., Pietzsch, T., Preibisch, S., Rueden, C., Saalfeld, S., Schmid, B., Tinevez, J.Y., White, D.J., Hartenstein, V., Eliceiri, K., Tomancak, P., Cardona, A., 2012. Fiji: an open-source platform for biological-image analysis. Nat. Methods 9, 676–682.

Selwitz, R.H., Ismail, A.I., Pitts, N.B., 2007. Dental caries. The Lancet 369, 51–59.

Sharma, P.K., Gibcus, M.J., van der Mei, H.C., Busscher, H.J., 2005a. Influence of fluid shear and microbubbles on bacterial detachment from a surface. Appl. Environ. Microbiol. 71, 3668–3673.

Sharma, P.K., Gibcus, M.J., Van Der Mei, H.C., Busscher, H.J., 2005b. Microbubble-induced detachment of coadhering oral bacteria from salivary pellicles. Eur. J. Oral Sci. 113, 326–332.

Shaw, T., Winston, M., Rupp, C.J., Klapper, I., Stoodley, P., 2004. Commonality of elastic relaxation times in biofilms. Phys. Rev. Lett. 93, 098102.

Sjogren, K., Lundberg, A.B., Birkhed, D., Dudgeon, D.J., Johnson, M.R., 2004. Interproximal plaque mass and fluoride retention after brushing and flossing – a comparative study of powered toothbrushing, manual toothbrushing and flossing. Oral Health Prev. Dent. 2, 119–124.

Stoodley, P., Cargo, R., Rupp, C.J., Wilson, S., Klapper, I., 2002. Biofilm material properties as related to shear-induced deformation and detachment phenomena. J. Ind. Microbiol. Biotechnol. 29, 361–367.

Stoodley, P., Nguyen, D., Longwell, M., Nistico, L., von Ohle, C., Milanovich, N., de Jager, M., 2007. Effect of the sonicare flexcare power toothbrush on fluoride delivery through *Streptococcus mutans* biofilms. Compend. Contin. Educ. Dent. 28, 15–22.

Towler, B.W., Rupp, C.J., Cunningham, A.B., Stoodley, P., 2003. Viscoelastic properties of a mixed culture biofilm from rheometer creep analysis. Biofouling 19, 279–285.

Waters, M.S., Kundu, S., Lin, N.J., Lin-Gibson, S., 2013. Microstructure and mechanical properties of in situ *Streptococcus mutans* biofilms. ACS Appl. Mater. Interfaces 6 (1), 327–332.

Wilking, J.N., Angelini, T.E., Seminara, A., Brenner, M.P., Weitz, D.A., 2011. Biofilms as complex fluids. MRS Bull. 36, 385–391.